

Source apportionment of PM_{2.5} at a regional background site in North China using PMF linked with radiocarbon analysis: Insight into the contribution of biomass burning

5 Zheng Zong^{1,6}, Xiaoping Wang², Chongguo Tian^{1,*}, Yingjun Chen^{3,*}, Lin Qu⁴, Ling Ji⁴, Guorui Zhi⁵,
Jun Li², Gan Zhang²

¹ Key Laboratory of Coastal Environmental Processes and Ecological Remediation, Yantai Institute of Coastal Zone Research, Chinese Academy of Sciences, Yantai, 264003, China

10 ² State Key Laboratory of Organic Geochemistry, Guangzhou Institute of Geochemistry, Chinese Academy of Sciences, Guangzhou, 510640, China

³ Key Laboratory of Cities' Mitigation and Adaptation to Climate Change in Shanghai (CMA), College of Environmental Science and Engineering, Tongji University, Shanghai, 200092, China

⁴ Yantai Oceanic Environmental Monitoring Central Station, SOA, Yantai, 264006, China

⁵ Chinese Research Academy of Environmental Sciences, Beijing, 100012, China

15 ⁶ University of Chinese Academy of Sciences, Beijing, 100049, China

* Corresponding author:

Chongguo Tian, Yantai Institute of Coastal Zone Research, CAS. Phone: +86-535-2109-160; Fax: +86-535-2109-000; e-mail: cgtian@yic.ac.cn

20 Yingjun Chen, College of Environmental Science and Engineering, Tongji University. Phone: +86-535-2109-160; Fax: +86-535-2109-000; e-mail: yjchentj@tongji.edu.cn

Abstract

Source apportionment of fine particles (PM_{2.5}) at a background site in North China in the winter of 2014 was made using statistical analysis, radiocarbon (¹⁴C) measurement, and Positive Matrix Factorization (PMF) modeling. Results showed that the concentration of PM_{2.5} was 77.6 ± 59.3 μg m⁻³, of which sulfate (SO₄²⁻) concentration was the highest, followed by nitrate (NO₃⁻), organic carbon (OC), elemental carbon (EC) and ammonium (NH₄⁺), respectively. Demonstrated by backward trajectory, more than half of the air masses during the sampling period were from the Beijing-Tianjin-Hebei (BTH) region, followed by Mongolia and the Shandong Peninsula. Cluster analysis of chemical species suggested an obvious signal of biomass burning in the PM_{2.5} from the Shandong Peninsula, while the PM_{2.5} from the BTH region showed a vehicle emission pattern. This finding was further confirmed by the ¹⁴C measurement of OC and EC in two merged samples. The ¹⁴C result indicated that biogenic and biomass burning emission contributed 59 ± 4% and 52 ± 2% to OC and EC concentrations, respectively, when air masses originated from the Shandong Peninsula, while the contributions fell to 46 ± 4% and 38 ± 1%, respectively, when the prevailing wind changed and came from the BTH region. The minimum deviation between source apportionment results from PMF and ¹⁴C measurement was adopted as the optimal choice of the model exercises. Here, two minor overestimates with the same range (3%) implied that the PMF result provided a reasonable source apportionment of the regional PM_{2.5} in this study. Based on the PMF modeling, eight sources were identified; of these, coal combustion, biomass burning, and vehicle emission were the main contributors of PM_{2.5}, accounting for 29.6%, 19.3% and 15.9%, respectively. Compared with overall source apportionment, the contributions of vehicle emission, mineral dust and coal combustion, biomass burning increased when air masses came from the BTH region, Mongolia, and the Shandong Peninsula, respectively. Since coal combustion and vehicle emission have been considered as the leading emission sources to be controlled for improving air quality, biomass burning was highlighted in the present study.

Keywords: Source apportionment, PMF, ¹⁴C measurement, PM_{2.5}

1 Introduction

In recent years, air pollution has become a top environmental issue in China, and the main concern is fine particulate matter less than 2.5 micrometers in diameter (PM_{2.5}) (Huang et al., 2014; Sheehan et al., 2014). Fine particulate aerosols have a strong adverse effect on human health, visibility, and directly or indirectly affect weather and climate (Pui et al., 2014; Chen et al., 2013; Lu et al., 2015; Tao et al., 2014b). The negative effects on public health, including damage to the respiratory and cardiovascular systems, the blood vessels of the brain, and the nervous system, have triggered both public alarm and official concern in China (Kessler, 2014). In response to this great concern, the Chinese government has introduced the Action Plan for Air Pollution Prevention and Control (2013–17), which aims at marked improvements in air quality until 2017. In the plan, the most strict regulation for improvement is a reduction of 25% in the annual average concentrations of PM_{2.5} by 2017 (Chinese-State-Council, 2013). It has been applied in North China because the region has become the most severely polluted area in China, characterized by increasingly frequent haze events and regional expansions of extreme air pollution (Hu et al., 2015; Boynard et al., 2014).

The key point in reducing PM_{2.5} concentrations is to control its sources. Reliable source identification and quantification are essential for the development of effective political abatement strategies. However, the sources of PM_{2.5} typically emit a mixture of pollutants, including gas and particle phases. They would mix further in the atmosphere and can undergo chemical transformations prior to impacting a specific receptor site, making it difficult to quantify the impacts (Balachandran et al., 2013). This encourages researchers to use more sophisticated techniques to quantify the contribution of individual sources to PM_{2.5} concentrations, such as the Positive Matrix Factorization (PMF) modeling (Paatero and Tapper, 1994), Chemical Mass Balance (CMB) modeling (Chow and Watson, 2002), organic tracers (Ding et al., 2013), and stable carbon isotopes (Cao et al., 2011). However, these different approaches often result in source contributions that can differ in magnitude and/or are poorly correlated, and the most reliable one cannot be determined (Balachandran et al., 2013). Radiocarbon (¹⁴C) measurement provides a powerful tool to unambiguously determine fossil and non-fossil sources of carbonaceous particles, and the method has been used in source apportionment of carbonaceous aerosols in China (Zhang et al., 2015; Liu et al., 2013; Liu et al., 2014). The underlying principle of ¹⁴C measurement is that radioisotope carbon has become extinct in fossil fuel due to its age (half-life 5730 years), while non-fossil carbon sources contain the

contemporary or near contemporary radiocarbon level (Szidat, 2009; Szidat et al., 2004). This method provides a more reliable source apportionment of PM_{2.5} by linking with other methods, although it focuses only on carbonaceous aerosols.

In the present study, source apportionment of PM_{2.5} at a regional background site in North China during winter was provided using PMF simulation, in which the source contribution of carbonaceous species was confirmed by the ¹⁴C measurement. The effort is vital for the development of efficient mediation policies to improve the air quality in North China. It is because regional source apportionment cannot be replaced by those extensively focused on the metropolitan areas such as Beijing (Zhang et al., 2013), Tianjin (Gu et al., 2011), Jinan (Gu et al., 2014), and others within North China. Thus, we collected continuous aerosol samples on Qimu Island during winter to apportion PM_{2.5} sources. The objectives of this study are (1) to determine the concentration burden and the chemical composition of PM_{2.5}, (2) to distinguish the source signals based on the chemical composition grouped according to the trajectory clusters, and (3) to apportion PM_{2.5} sources using the PMF model linked with ¹⁴C measurement.

2 Materials and methods

2.1 Sampling site and sample collection

The sampling campaign was conducted from January 3 to February 11, 2014, at the Longkou Environmental Monitoring Station of the State Ocean Administration of China (37 °41 N, 120 °16 E), on Qimu Island. The island extends to the Bohai Sea westwards, and is surrounded by sea on its other three sides, as shown in Fig. 1. The sampling site is located approximately 15 km northwest of the Longkou urban district and 300 km southeast of the Beijing-Tianjin-Hebei (BTH) region. Longkou city is closest to the sampling site, and emissions from the city can be considered the primary local sources.

A total of 76 PM_{2.5} samples were collected continuously on quartz fiber filters (Whatman, QM-A, 20.3 × 25.4 cm², heated at 450 °C for 6 h before use) using a Tisch high volume sampler at a flow rate of 1.13 m³ min⁻¹ during the sampling period. The duration for each sample was 12 h, from 06:00–18:00 and from 18:00–06:00 (local time) the next day. Before and after each sample, quartz fiber filters were subjected to 24 h equilibration at 25 ± 1 °C temperature and 50 ± 2% relative humidity, and were then analyzed gravimetrically using a Sartorius MC5 electronic microbalance (Zhang et al., 2015; Liu et al., 2013; Huang et al., 2014). Each filter was weighed at least three times.

Acceptable difference among the repetitions was less than 10 µg for a blank filter and less than 20 µg for a sampled filter. After weighing, loaded filters were stored in a refrigerator at -20 °C until chemical analysis. In addition, field blank filters were collected to subtract possible contamination occurring during or after sampling.

5 2.2 Chemical analysis

2.2.1 OC and EC

Organic carbon (OC) and elemental carbon (EC) were analyzed by a Desert Research Institute (DRI) Model 2001 Carbon analyzer (Atmoslytic Inc., Calabasas, CA) following the Interagency Monitoring of Protected Visual Environment (IMPROVE_A) thermal/optical reflectance (TOR) protocol (Chow et al., 2007). A punch of 0.544 cm² from each quartz filter was heated to produce four fractions (OC1, OC2, OC3 and OC4) in four temperature steps (140, 280, 480, 580 °C) under a non-oxidizing helium atmosphere and then in 2% O₂/98% He atmosphere at 580 °C (EC1), 740 °C (EC2), and 840 °C (EC3) for the EC fractions. At the same time, pyrolyzed organic carbon (POC) was produced in the inert atmosphere, which decreased the reflected light to correct for charred OC.

15 The concentrations of OC and EC were obtained according to the IMPROVE protocol, $OC = OC1 + OC2 + OC3 + OC4 + POC$ and $EC = EC1 + EC2 + EC3 - POC$. The detection limits of the method for OC and EC were 0.82 and 0.20 µg cm⁻², respectively. In addition, blank filters and replicate samples were examined simultaneously after analyzing a batch of 10 samples to obtain inherent OC and EC concentrations on the filters and to evaluate measurement accuracy, respectively. In this

20 study, the contributions of OC and EC from blank filters were < 3.5 and 0.6% of their respective average concentrations. The uncertainties of OC (5.6%) and EC (5.5%) were calculated from the replicate measurements.

2.2.2 Water-soluble ions and metal elements

Two 47 mm diameter punches were cut off from each quartz fiber filter, one of which was

25 subjected to Milli-Q water extraction for ionic measurement, and the other underwent induced acid digestion for elemental measurement. The concentrations of water soluble ions: sodium (Na⁺), ammonium (NH₄⁺), potassium (K⁺), magnesium (Mg²⁺), calcium (Ca²⁺), chlorine (Cl⁻), nitrate (NO₃⁻) and sulfate (SO₄²⁻), were determined by ion chromatograph (Dionex ICS3000, Dionex Ltd., America) based on the analysis method (Shahsavani et al., 2012). The concentrations of metal elements:

30 titanium (Ti), vanadium (V), manganese (Mn), ferrum (Fe), cobalt (Co), nickel (Ni), cuprum (Cu),

zinc (Zn), arsenic (As), cadmium (Cd) and plumbum (Pb), were estimated via inductively coupled plasma mass spectrometry (ICP-MS of ELAN DRCII type, Perkin Elmer Ltd., Hong Kong) following the previous method (Wang et al., 2006). The detection limit of water-soluble ions was 10 ng ml⁻¹ with error < 5%, and 1 ml RbBr of 200 ppm was put in the solution as an internal standard before analysis. The resolution of ICP-MS ranged from 0.3 to 3.0 amu with a detection limit < 0.01 ng ml⁻¹, and error < 5%. Five ppb elemental indium (In) was put in the solution before analysis as an internal standard.

2.2.3 ¹⁴C measurement

To achieve more ¹⁴C information on carbonaceous fractions in PM_{2.5}, OC was split into water-soluble organic carbon (WSOC) and water-insoluble organic carbon (WIOC) fractions. WSOC was extracted from a punch filter by Milli-Q water as described in a previous study (Zhang et al., 2014c), and was quantified as total dissolved organic carbon in solution by a total organic carbon (TOC) analyzer (Shimadzu TOC-VCPH, Japan). WIOC was quantified by OC given by the TOR protocol subtracting WSOC. Two combined samples reflecting source signals from the Shandong Peninsula (M1) and the BTH region (M2), respectively, were selected for ¹⁴C measurement. The uncertainties of WSOC calculated from four time measurements were 6.7% for M1 and 5.3% for M2, while the uncertainties of WIOC were 8.7% and 7.7%, in sequence, estimated by error propagation formulas.

¹⁴C measurement of WSOC, WIOC and EC was performed using the OC/EC separation system (Liu et al., 2014). Briefly, the extracted Milli-Q water was freeze-dried, and the residue was re-dissolved and transferred to a pre-combusted quartz tube. Then the quartz tube was combusted at 850 °C, making WSOC convert into CO₂. The extracted filters were isolated at 340 °C for 15 min for WIOC, after a flash heating of 650 °C for 45 s to minimize charring. After separation, the filters were heated at 375 °C for 4 h to remove charring, and then oxidized under a stream of pure oxygen at 650 °C for 10 min to analyze the EC fraction. Finally, the corresponding evolving CO₂ (WSOC, WIOC and EC) was cryo-trapped and reduced to graphite at 600 °C for accelerator mass spectrometry (AMS) target preparation with the sealed tube zinc reduction method (200 mg, Alfa Aesar, 1.5-3 mm, 99.99%) (Xu et al., 2007; Zhang et al., 2010; Wacker et al., 2013). The preparation of graphite targets for AMS analysis was performed using the graphitization line at the Guangzhou Institute of Geochemistry, CAS. The ratios of ¹⁴C/¹²C in the graphite samples were determined

through a NEC compact AMS at Peking University, which sensitivity was less than 6×10^{-15} and the precision of ^{14}C measurement for the samples was better than 0.5%.

Generally, ^{14}C results were expressed as fractions of modern carbon (f_m), which is larger than 1 due to the nuclear bomb in 1950s and 1960s. It includes biogenic and biomass burning ($f_{m,\text{bio}}$, $f_{m,\text{bb}}$, respectively) and was estimated to be 1.06 ± 0.015 and 1.13 ± 0.05 for $f_{m,\text{bio}}$ and $f_{m,\text{bb}}$, respectively. Of them, $f_{m,\text{bio}}$ value was estimated from long term series of $^{14}\text{CO}_2$ measurement at Schauinsland station (Levin et al., 2010), while $f_{m,\text{bb}}$ was estimated by a tree-growth model (Mohn et al., 2008). In this study, f_m (EC) equals $f_{m,\text{bb}}$ assuming biomass burning is the only non-fossil source for EC, while f_m (OC) is adopted as the average value of $f_{m,\text{bio}}$ and $f_{m,\text{bb}}$ given OC originated equally from biogenic and biomass burning emission. Finally, conversion factors were determined to be 1.10 and 1.06 for EC and OC (Liu et al., 2014), respectively, considering the steadily decline of ^{14}C after the factors estimation. So the fraction of contemporary carbon (f_c) values in the samples were defined as $f_c = f_m/1.10$ for EC, $f_c = f_m/1.06$ for OC, and the fraction of fossil (f_f) was defined as $f_f = 1 - f_c$ (Zong et al., 2015). In this study, the isolated carbon amounts were typically in the range of 120-280 μg , depending on the samples. The WSOC and WIOC in the blank samples only accounted for 1.9% and 1.2%, respectively, of the average value of M1 and M2. EC was not found in the blank samples. Thus, the blank interference for f_m of M1 and M2 in the ^{14}C measurement was very small and was ignored in this study.

2.3 Data analysis methods

The hybrid single-particle Lagrangian integrated trajectory (HYSPLIT) model was used to generate 48-h backward trajectories with 12 h intervals. The HYSPLIT model is available on the National Oceanic and Atmospheric Administration Air Resource Laboratory website (www.arl.noaa.gov/ready/hysplit4.html). The trajectories were calculated for air masses starting from the sampling site at 500 m above ground level. A total of 152 trajectories were generated and these trajectories were bunched into three clusters by the clustering function in the HYSPLIT model. Air masses from the BTH region, Mongolia and the Shandong Peninsula were defined as clusters from 1 to 3, respectively, as shown in Fig. 1. In order to follow the clusters corresponding to region information, region abbreviation, such as BTH, MON, SDP for the BTH region, Mongolia and the Shandong Peninsula, respectively, was introduced as supplementary in the text. The observed chemical components of $\text{PM}_{2.5}$ from the three clusters were compared with each other to assess their

potential sources.

PMF v5.0 was utilized to apportion PM_{2.5} sources, which is available at the US EPA website: www.epa.gov/air-research/positive-matrix-factorization-model-environmental-data-analyses. PMF is a multivariate factor analysis tool, which assumes that concentrations at a receptor site are supported by linear combinations of different source emissions. Thus, measured mass concentrations of selected species can be mostly expressed as (Paatero et al., 2014):

$$x_{ij} = \sum_{k=1}^p g_{ik} f_{kj} + e_{ij} \quad (1)$$

where x_{ij} is the measured concentration of the j^{th} species in the i^{th} sample, f_{kj} is the profile of j^{th} chemical species emitted by the k^{th} source, g_{ik} is the amount of mass contributed by k^{th} source to the i^{th} sample, and e_{ij} is the residual for each samples/species. The matrices of g and f are determined by minimizing an objective function (Paatero et al., 2014).

To further confirm PM_{2.5} sources apportioned by PMF model, the source contributions of OC and EC were examined by ¹⁴C measurement. The modeled source contributions were merged into two groups according to fossil and contemporary carbon sources. Then the contribution fractions of fossil or contemporary carbon sources to OC and EC could be compared with the ¹⁴C measurement for specified samples as:

$$R_{ij} = \frac{\sum_{k=1}^n g_{ik} f_{kj}}{\sum_{k=1}^p g_{ik} f_{kj}} \quad (2)$$

where R is the contribution fraction, and matrices of g and f are the same as in eqn.(1). The subscript i is a specified sample, j is OC or EC species. n is the number of fossil or contemporary carbon sources, and p is the number of all sources. The minimum deviation of PM_{2.5} source contributions apportioned by the PMF exercise and ¹⁴C measurement was used to determine the final model scenario. The verified model result can be regarded as providing a more reliable solution for the source apportionment.

2.4 Principle of samples selected for ¹⁴C analysis

The comparison of OC and EC focused on cluster 1 (BTH) and cluster 3 (SDP). It was due to most species of PM_{2.5} in the two clusters were statistically greater than in cluster 2 (MON), as

elaborated later. Besides, ^{14}C measurement result was an important parameter for source comparison in the two clusters. So for better comparison using a few samples for expensive ^{14}C analysis, the representative capacity of all samples in the two clusters was examined thoroughly. Generally, PMF can better interpret those data close to the average condition of each chemical species. Since the method utilizes error-minimizing estimates to decompose a matrix of sample data into two matrices, which usually under strict non-negativity constraints for the factors (Paatero et al., 2014). Therefore, OC and EC concentrations, and ratios of OC/PM_{2.5} and EC/PM_{2.5} of each sample, were compared with those in the corresponding cluster by mean test. In addition, the concentration, area passed through, etc. of independent samples were considered greatly when picking them for ^{14}C measurement.

Finally, two combined samples were selected from a perfect synoptic process during the sampling period. The synoptic process occurred during January 16th and 18th, 2014. As shown in Fig. 2, the first half of air masses in the synoptic process were derived from the south and passed through the Shandong Peninsula (cluster 3) and the bottom half were from the north and passed over the BTH region (cluster 1). Thus, two samples collected continually from 06:00 to 18:00, January 16th and from 18:00 to 06:00 the next day in the first half of the synoptic process were merged into one sample (M1) for the ^{14}C analysis. Similarly, other two samples collected continually from 18:00 to 6:00, January 17th and from 06:00 to 18:00 in the next day were combined into the other sample (M2). M1 reflected the signal of air masses coming from the Shandong Peninsula, while M2 showed the pattern of air masses from the BTH region. Mean test showed that except for a significant high ratio of EC/PM_{2.5}, the OC and EC concentrations and the OC/PM_{2.5} ratio of M2 were negligibly different from cluster 1, at a 95% significance level. It indicated its perfect representative capability for further carbonaceous analysis. However, M1 may have slight lower representativeness. Since only ratios of OC/PM_{2.5} and EC/PM_{2.5} had no statistical difference, OC and EC concentrations were relative higher than that in the cluster 3 at the same significance level. Even so, the samples were still considered for ^{14}C analysis because they were from a faultless synoptic process during the sampling period. Continuous samples were more dramatic than insular samples. In addition, the insignificant difference of the ratios of OC/PM_{2.5} and EC/PM_{2.5} assured the validity for PM_{2.5} source assessment, which was more important than concentration in this study.

3 Results and discussion

3.1 General characteristics of PM_{2.5} and chemical components

Table S2 lists a statistical summary of the concentrations of PM_{2.5}, water-soluble ions, carbonaceous species and metal elements during the sampling period. As shown, the mean concentration of PM_{2.5} was $77.6 \pm 59.3 \mu\text{g m}^{-3}$, which was more than two times higher than the grade I national standards ($35 \mu\text{g m}^{-3}$, Ministry of Environmental Protection of China: GB 3095-2012, www.zhb.gov.cn, 2012-02-29). Although the level of PM_{2.5} concentration on Qimu Island was higher than the national standard, it was much lower than that observed in winter in the megacities of North China, such as in Beijing ($208 \mu\text{g m}^{-3}$ of PM_{2.1} in 2013) (Tian et al., 2014) and Tianjin ($221 \mu\text{g m}^{-3}$ in 2013) (Han et al., 2014).

The relative contribution of species for PM_{2.5} is displayed in Fig. 3. Generally, water-soluble inorganic species (WSIS) were the dominant species, accounting for $43 \pm 16\%$ of PM_{2.5} mass concentrations. Among the ions, SO_4^{2-} ranked the highest with a mean concentration of $14.2 \pm 18.0 \mu\text{g m}^{-3}$, followed by NO_3^- ($11.9 \pm 16.4 \mu\text{g m}^{-3}$) and NH_4^+ ($3.11 \pm 2.14 \mu\text{g m}^{-3}$). The sum of the three secondary inorganic aerosols constituted the majority ($88 \pm 12\%$) of the total WSIS concentrations. In addition, the average concentrations of OC and EC were 6.85 ± 4.81 and $4.90 \pm 4.11 \mu\text{g m}^{-3}$, accounting for $8.8 \pm 2.1\%$ and $6.3 \pm 1.8\%$ of the PM_{2.5} concentrations, respectively. Total concentrations of analyzed metal elements were $665 \pm 472 \text{ ng m}^{-3}$, accounting for $0.86 \pm 0.50\%$ of the PM_{2.5}. Among the measured metal elements, the concentration of Fe ($408 \pm 285 \text{ ng m}^{-3}$) was the highest, followed by Zn ($107 \pm 142 \text{ ng m}^{-3}$), and Pb ($88.4 \pm 85.7 \text{ ng m}^{-3}$).

At the sampling site, the organic matter was clearly lower but the relative contributions of SO_4^{2-} , NO_3^- , and NH_4^+ to the PM_{2.5} were significantly higher than those in the cities within North China, such as Beijing and Tianjin (Zhang et al., 2013; Zhao et al., 2013; Tian et al., 2016). The high contributions of SO_4^{2-} , NO_3^- , and NH_4^+ agree with the regional scale emissions of their precursors in North China, as it has been reported that SO_2 , NO_x , and NH_3 emissions were approximately 10, 5, and 5 times higher compared to OC in the region, respectively (Zhao et al., 2012). This finding was also in agreement with results measured at Changdao Island (Feng et al., 2012), which is located at the demarcation line between the Bohai Sea and the Yellow Sea and is a popular resort with little industry approximately 7 km north of the Shandong Peninsula (Feng et al., 2012). Measurements at the island were interpreted as the indicative patterns of atmospheric outflow and regional pollution in North China (Feng et al., 2012; Feng et al., 2007). It suggested that our measurements also provide a

regional signal of PM_{2.5} pollution in North China. Furthermore, SO₄²⁻ was the largest contributor of PM_{2.5}, and this characteristic is usually regarded as a regional pollution signal in winter. This is because there is a lack of a fast conversion rate of SO₂ to SO₄²⁻ in clouds or aerosol droplets and oxidation reactions via OH free radicals under low temperature conditions in PM_{2.5} source areas (Hu et al., 2015). Thus, our measurement largely reflected a pollution pattern on a regional scale, rather than just in source areas.

3.2 Source signals based on cluster analysis

As shown in Fig. 1, the 48-h back trajectory clusters indicate that more than half of the air masses (54%) during the sampling period were from the BTH region, followed by the air masses from Mongolia (35%). Air masses of these two types traveled about 200 and 250 km, respectively, over the Bohai Sea before arriving at the sampling site. Thus, the atmospheric pollutants carried by the two kinds of air masses were mixed well during transport, creating regional pollution signals. Only a small part of the air masses (11%) was from the Shandong Peninsula, potentially reflecting a mixed contribution of local and regional sources from south area of the sampling site. In addition, only one trajectory in cluster 3 (SDP) passed the urban area of Longkou, when PM_{2.5} concentration was measured at 95.3 μg m⁻³. This level was lower than the average of PM_{2.5} concentrations in cluster 3, indicating minor contribution of local source emissions. In order to reveal the pollution patterns and source signals of PM_{2.5} carried by air masses from the three different regions, chemical species of PM_{2.5} were grouped according to the three trajectory clusters, as listed in Table 1.

Generally, mean test showed that the concentration levels and most abundant species types of PM_{2.5} in clusters 1 (BTH) and 3 (SDP) are both insignificantly different ($p > 0.05$) and statistically higher than in cluster 2 (MON) ($p < 0.01$), as shown in Table 1. The patterns observed are consistent with the spatial distributions of their emissions and concentrations in North China; as reported, there are higher emissions and more severely pollution in the BTH region and Shandong Province than in Inner Mongolia and Liaoning (Zhao et al., 2012; Yang et al., 2011). Compared with the Shandong Peninsula, the pollution in BTH region may be even worse because it travels much longer distances to the sampling site, yet the difference of the PM_{2.5} concentrations attributed to the two areas are trivial. In addition, the mean wind speed of cluster 2 (MON) was 7.60 m s⁻¹, which was dramatically higher than that of cluster 1 (BTH) (4.79 m s⁻¹) and cluster 3 (SDP) (4.86 m s⁻¹). Wind speeds were determined by averaging hourly moving distances of air masses during a 48 h period. The higher

wind speed of cluster 2 might partly contribute to the lower PM_{2.5} level at sampling site, since high wind speed could provide favorable diffusion conditions for atmospheric pollutants.

Some anomalies compared with previous discussion provided different source signals amongst the clusters. For instance, K⁺ concentration was significantly higher in cluster 3 (SDP) than in cluster 1 (BTH), while the Ti concentration was obviously lower. This reflected relatively high emissions of K⁺ in the Shandong Peninsula and Ti in the BTH region from both natural sources and anthropogenic activities. Likewise, the concentration of Na⁺ in cluster 2 (MON) was much higher than in clusters 1 and 3, showing a large contribution from sea salt particles generated by sea spray under high wind speed to PM_{2.5} concentrations. This suggested that sea salt sources should not be ignored in this study because of the proximity of the sampling site to the Bohai Sea.

Sea salt emissions are comprised of Cl⁻, SO₄²⁻, Na⁺, K⁺, Mg²⁺ and Ca²⁺ (Ni et al., 2013). The amounts of different chemical species in sea salt emissions can be determined using Na⁺ as the tracer of sea salt; the amounts of these species from non-sea salt (nss-) emissions can be expressed as:

$$nss-x = x - [Na^+] \times a \quad (3)$$

where x indicates the Cl⁻, SO₄²⁻, K⁺, Mg²⁺ and Ca²⁺ concentrations, and a is the typical equivalent concentration ratio of the corresponding species to Na⁺ in average seawater: Cl⁻/Na⁺ (1.80), SO₄²⁻/Na⁺ (0.250), K⁺/Na⁺ (0.036), Mg²⁺/Na⁺ (0.120) and Ca²⁺/Na⁺ (0.038) (Ni et al., 2013). If the calculated concentration of non-sea salt chemical species is negative, then no excess species exist. According to the calculation, for corresponding total chemical concentration levels grouped in clusters from 1 (BTH) to 3 (SDP), nss-Cl⁻ accounted for 55 ± 29%, 19 ± 24% and 77 ± 10% of total Cl⁻; nss-SO₄²⁻ accounted for 99 ± 2%, 95 ± 4% and 99 ± 0.3% of total SO₄²⁻; nss-K⁺ accounted for 98 ± 3%, 89 ± 9% and 99 ± 0.3% of total K⁺; nss-Ca²⁺ accounted for 95 ± 4%, 91 ± 10% and 96 ± 3% of total Ca²⁺. Thus, marked contributions of nss-emission sources to chemical concentrations at all three clusters were found. However, these values may be underestimated, since total Na⁺ concentrations do not necessarily originate from sea salt alone, but could partially come from dust and burning sources (Zhang et al., 2013). In addition, the loss of Cl⁻ particles due to a chloride depletion mechanism further supports the underestimation of Cl⁻. The contributions of nss-sources were lower in cluster 2 (MON) than in clusters 1 (BTH) and 3 (SDP), which was attributed to the high emissions of sea spray coupled with high wind speed in cluster 2. Generally, K⁺ is often used as

a tracer for biomass burning. The high K^+ concentration and the largest contribution of $nss-K^+$ in cluster 3 (SDP) indicated a clear high emission associated with agricultural burning in the Shandong Peninsula. This finding agreed with the fact that Shandong province is the largest producer of crop residues in North China (Zhao et al., 2012), and biomass burning is an important source of inorganic and organic aerosols in the Bohai sea atmosphere (Feng et al., 2012; Wang et al., 2014). The contribution of $nss-Mg^{2+}$ to total Mg^{2+} concentration was less than 4% for the all clusters, indicating the specie came mostly from sea salt emission. The mass ratio of Mg^{2+} to Na^+ was 0.07 ± 0.06 , 0.06 ± 0.03 and 0.06 ± 0.03 for clusters from 1 to 3, respectively. The ratios were less than 0.23, also demonstrating that Mg^{2+} mainly came from sea salt source (Zhang et al., 2013).

The ratios of OC/EC and $NO_3^-/nss-SO_4^{2-}$ were used as tracers to assess source signals of the three clusters. Low temperature burning, such as agricultural residue burning, emits more OC compared with high temperature burning, e.g. vehicle exhaust (Gibson et al., 2013; Cui et al., 2016). Thus, the ratio of OC/EC is often used to evaluate relative contributions of low and high temperature burning emission (Zhao et al., 2012). The OC/EC ratios were 1.41 ± 0.30 , 1.47 ± 0.29 and 2.14 ± 0.50 for clusters 1 to 3, respectively. Mean test showed that the difference between cluster 1 (BTH) and cluster 2 (MON) ratios were insignificant at a 95% confidence level, and both of them were statistically lower compared with that of cluster 3 (SDP) at the same confidence level. This suggests that low temperature burning contributed clearly to the emission in cluster 3 (SDP), while high temperature burning emission was more distinct in clusters 1 (BTH) and 2 (MON). Furthermore, mobile sources, such as vehicles, exhaust more NO_x than SO_2 , while stationary sources, such as coal-fired power plants, emit more SO_2 than NO_x (Wang et al., 2005). These two precursors convert into SO_4^{2-} and NO_3^- in the atmosphere, and the two type sources show different ratios of NO_3^-/SO_4^{2-} . Hence, this ratio is usually adopted as an indicator of the relative importance of mobile versus the stationary sources of sulfur and nitrogen in the atmosphere (Zhao et al., 2013; Liu et al., 2014). After deducting the contribution of sea salt to SO_4^{2-} , the mean ratios of $NO_3^-/nss-SO_4^{2-}$ were 0.96 ± 0.31 , 0.47 ± 0.24 and 0.64 ± 0.14 for clusters 1 to 3, respectively. Mean test showed that the three cluster ratios exhibit significant differences from each other at a 95% confidence level. The highest ratio in cluster 1 (BTH) suggests that mobile sources are the most important contributors in the BTH region, followed by the Shandong Peninsula (cluster 3). The ratio of $NO_3^-/nss-SO_4^{2-}$ in cluster 1 was within the range of those found in large cities, such as Beijing (1.20), Tianjin (0.73), and Shijiazhuang

(0.76), the capital of Hebei province (Zhao et al., 2013), reflecting a hybrid contribution from the BTH region. The value in cluster 2 (MON) was slightly lower than that in winter in Chengde (0.55), a city located in the northern mountainous area of Hebei Province (Zhao et al., 2013). It indicated more obvious contribution of stationary source emissions in areas such as eastern Inner Mongolia and the west part of Liaoning, than the BTH region and the Shandong Peninsula. In addition, these stationary source emissions are possibly associated with coal combustion because of the lower OC/EC ratio in cluster 2 (MON) compared to cluster 3 (SDP).

3.3 Source apportionment of carbonaceous PM_{2.5}

The cluster analysis indicated that PM_{2.5} concentrations increased significantly when air masses came from the BTH region and the Shandong Peninsula during the sampling period. The chemical species in PM_{2.5} from the BTH region possessed a clear signal of high temperature burning and mobile sources, while those from the Shandong Peninsula had more obvious patterns of low temperature burning and stationary sources.

Table 2 lists the concentrations and contemporary carbon fractions of OC, WSOC, WIOC and EC of the two combined samples, which were selected via a perfect synoptic process during the sampling period. The fraction of OC was yielded by the average weights of concentrations of WSOC and WIOC fractions. It can be expressed as:

$$f_c(\text{OC}) = [f_c(\text{WSOC}) \times c(\text{WSOC}) + f_c(\text{WIOC}) \times c(\text{WIOC})] / [c(\text{WSOC}) + c(\text{WIOC})] \quad (4)$$

where $f_c(\text{OC})$, $f_c(\text{WSOC})$ and $f_c(\text{WIOC})$ are the contemporary carbon fractions of OC, WSOC and WIOC, and $c(\text{WSOC})$ and $c(\text{WIOC})$ are the concentrations of WSOC and WIOC, respectively. Generally, WSOC is mainly associated with biomass burning and secondary formation (Du et al., 2014), while OC directly emitted from the combustion of fossil fuel is mostly water insoluble (Weber et al., 2007). During the earlier stage of the synoptic process, the concentrations of WSOC and WIOC were $6.42 \pm 0.41 \mu\text{g m}^{-3}$ and $6.30 \pm 0.62 \mu\text{g m}^{-3}$, respectively. Later on, the concentrations of the two carbonaceous fractions fell to $3.70 \pm 0.20 \mu\text{g m}^{-3}$ and $5.31 \pm 0.40 \mu\text{g m}^{-3}$, respectively, after the shift of the dominant wind direction from southerly to northwesterly, as shown in Fig. 2. The fraction of WSOC to OC decreased from $50 \pm 3\%$ to $41 \pm 3\%$ and the WIOC fraction increased from $50 \pm 4\%$ to $59 \pm 6\%$ before and after the shift of the dominant wind direction. This suggested that the contribution of fossil fuel combustion was more obvious in the BTH region than in the Shandong Peninsula. The contemporary carbon fractions of WSOC and WIOC decreased from 0.59 ± 0.04 to

0.49 ± 0.03 and from 0.60 ± 0.03 to 0.43 ± 0.03, respectively, which indicated a decrease in the impact of biogenic and biomass burning emission and an increase in contribution of fossil fuel combustion to the two OC fractions. After the weighted average of the WSOC and WIOC fractions, the $f_c(\text{OC})$ values were 0.59 ± 0.04 and 0.46 ± 0.04 for the M1 and M2 samples, respectively.

5 Together with $f_c(\text{EC})$, we determined that biogenic and biomass burning emission contributed 59 ± 4% of OC and 52 ± 2% of EC concentrations, respectively, when air masses were from the Shandong Peninsula. After the change of wind direction, the contribution of biogenic and biomass burning emission fell to 46 ± 4% for OC and 38 ± 1% for EC, respectively, which suggested that fossil fuel combustion contributed a dominant portion of the carbonaceous aerosols from the BTH region.

10 The synoptic process clearly showed a shift of the dominant wind from southerly to northwesterly, namely from the Shandong Peninsula to the BTH region. Meanwhile, the pattern of biogenic and biomass burning emission became more and more weakly, and the signal of fossil fuel combustion became more and more obvious. This was in agreement with our previous discussion. For instance, emissions in the BTH region exhibited more signals of high temperature burning and
15 vehicle exhaust. It was characterized by the lower ratio of OC/EC (1.41 ± 0.30), the higher ratio of $\text{NO}_3^-/\text{nss-SO}_4^{2-}$ (0.96 ± 0.31), and the relatively lower concentration of nss-K^+ compared with those in the Shandong Peninsula (2.14 ± 0.50 for OC/EC ratio, 0.64 ± 0.14 for $\text{NO}_3^-/\text{nss-SO}_4^{2-}$ ratio). The contribution of the biogenic and biomass burning emission to carbonaceous aerosols in the Shandong Peninsula was still significant, which has often been mentioned in previous studies (Feng et al., 2012;
20 Zong et al., 2015; Wang et al., 2014), although there was great combustion of fossil fuel (e.g., coal) for not only industrial activity but also heating in winter.

3.4 Source apportionment of $\text{PM}_{2.5}$

The EPA PMF 5.0 model was used together with a data set of 76×22 (76 samples with 22 species) to further quantitatively estimate the source contributions of $\text{PM}_{2.5}$ (Bressi et al., 2014; Choi et al., 2013). After iterative testing from 5 to 15 factors in model exercises, we found the minimum deviation of the source apportionment of OC and EC between the results from ^{14}C measurement and a PMF model scenario with an F_{peak} value of 0 and the lowest Q values (6245). In addition, the model uncertainty was also explored as shown in text S1 in the supplement.

Based on PMF modeling results, eight source factors were identified, as shown in Fig. 4. Traffic
30 emission has attracted considerable concern in the megacities of China (e.g., Beijing and Shanghai)

due to the remarkable growth of vehicle numbers in China (Jing et al., 2016; Zheng et al., 2014). In Beijing in 2012, on-road vehicles were estimated to be the largest local emission source and contributed 22% of PM_{2.5}, including primary and secondary fine particles but vehicle-induced road dust (Zhang et al., 2014b). The first source factor was characterized by high loadings of NO₃⁻, SO₄²⁻, NH₄⁺, OC, EC, Zn and Cu, which matched a vehicle emission profile (Zhang et al., 2013). Generally, NO₃⁻, SO₄²⁻, OC and EC are mainly from engine exhaust emissions (Dorado et al., 2003), and NH₄⁺ is from vehicles equipped with three-way catalytic converters (Chang et al., 2016). Not only Zn and Cu, but also Pb and Cd are emitted directly bounded particles from exhaust (Tan et al., 2014). In addition, the high NO₃⁻/SO₄²⁻ ratio of 1.28 calculated by the PMF result suggested high temperature burning and vehicle emissions (Gelencser et al., 2007). This source was the largest contributor of NO₃⁻, which contributed 41% during the sampling period. The contribution was higher than 31% of NO_x emitted by traffic sectors in North China in 2003, an expected increase of the contribution due to the rapid rise of vehicles in North China in recent years (Shi et al., 2014b). This factor was the prevalent anthropogenic PM_{2.5} source in North China, with an average contribution of 16% during the sampling period. The contribution was lower than that in Beijing (Zhang et al., 2014b), agreeing with the regional contribution characteristic in our study, rather than ones in large cities (Zhou et al., 2016). The second factor consisted of mineral dust elements, such as Mn, Fe and Co, and chemical species from human activities, such as Zn and EC (Khan et al., 2016), showing a mixed pattern of natural and anthropogenic emissions. Vehicle emission is an important source of atmospheric Zn pollution, because it can be emitted from direct exhaust, lubricating oil additives, tire and brake abrasion, wearing and corrosion from anticorrosion galvanized automobile sheet, and re-entrainment dust enriched with Zn (Duan and Tan, 2013). Thus, the source factor was identified as traffic dust under the relative high contribution of vehicle emission to PM_{2.5} concentration.

The third source factor was ship emissions, typically characterized by high proportions of Ni and V, and a high V/Ni ratio (Cappa et al., 2014). High loading of these two metals is typically associated with emissions from residual oil, probably derived from shipping activities and some industrial processes (Pey et al., 2013). In addition, a V/Ni ratio of more than 0.7 is always considered a sign of PM_{2.5} influenced by shipping emissions (Zhang et al., 2014a). The average ratio of V/Ni from the measured data was 0.93 ± 0.46 , indicating an obvious contribution of shipping emission. The average ratio of V/Ni calculated from the PMF source profile was 1.02, which was the second

highest value amongst those derived from the eight sources. The highest value of 1.29 was for the mineral dust source, agreeing with a high ratio of 3.06 for soil background concentrations of the two metals in mainland China (Pan et al., 2013).

The fourth factor showed high loadings of Cu, Zn, As, Cd and Pb, which were treated as signals of industrial processes (Amil et al., 2016). Emissions from the iron and steel industry are possibly important amongst those industrial processes for two reasons. One is that the sintering process in the iron and steel industries emits large amounts of Pb, Hg, Zn and other heavy metal pollutants, and other processes such as ironmaking and steelmaking also emit fugitive dust containing high concentrations of heavy metals (Duan and Tan, 2013). The other reason is the huge scale of steel production in North China. National statistical data shows that China produced approximately half the world's production of crude steel in 2014, and production in the BTH and Shandong province were 25.3% and 7.8%, respectively, of the total amount in China, respectively, which is available at the website (<http://www.stats.gov.cn/tjsj/ndsj/>). Thus, iron and steel industries are likely the main atmospheric sources of the metal elements in this study. In addition, the contribution of the source to SO_4^{2-} was 12%, which was similar to previously reported contributions of industrial processes to the amount of sulfur dioxide (15%) (Zhao et al., 2012).

The fifth source factor was biomass burning, characterized by high concentrations of K^+ , OC, EC and NH_4^+ , which have been used extensively as tracers of biomass-burning aerosols (Zhou et al., 2015; Tao et al., 2014a). The contribution of this source was significantly higher in cluster 3 (SDP) than in clusters 1 (BTH) and 2 (MON), as listed in Table 3. Results agreed with more biomass burning emission in the Shandong Peninsula, characterized by rich K^+ and the high OC/EC ratio (Zong et al., 2015). The average ratio of OC to EC from this source was also the highest (1.84) amongst the eight identified sources (0.23-1.84) calculated by the PMF modeling.

The sixth source factor was mineral dust, characterized typically by crustal elements, such as Ca^{2+} , Ti and Fe, which are often used as markers of soil dust (Zhang et al., 2013). The contribution of this source was obviously higher in cluster 2 (MON) than that in clusters 1 (BTH) and 3 (SDP), corresponding to the high wind speed in it. The average ratio of OC to EC (1.53) from this source was obviously higher than that (0.23) from vehicle dust, possibly suggesting that the source contributed more OC, mainly derived from biogenic dust, such as plant debris.

The seventh source factor was characterized by high loadings of Cl^- , Na^+ , OC, EC, SO_4^{2-} Ni and

As. Coal combustion is often indicated by elevated Cl^- linked with high Na^+ , OC and EC (Zhang et al., 2013). This source was the largest contributor of SO_4^{2-} in the present study, matching with the inventory results in North China (Zhao et al., 2012). In addition, this source was the largest contributor of $\text{PM}_{2.5}$, as listed in Table 3, which agreed with the fact that coal combustion is the predominant source of fine particle aerosols over China (Pui et al., 2014). High loadings of As and Ni in the factor was also used as a marker for coal-fired power plant emissions (Tan et al., 2016).

The last source factor was sea salt, characterized by high loadings of Na^+ , Mg^{2+} and Cl^- , which are related to the primary sea-salt aerosols produced by mechanical disruption of the ocean surface (Gupta et al., 2015). Similarly to the second source (mineral dust), high wind speed in cluster 2 (MON) made the contribution of this source in it higher than that in clusters 1 (BTH) and 3 (SDP). In addition, the higher contribution fraction of Mg^{2+} compared to Cl^- in this source was in agreement with our previous discussion. The concentration ratios of Cl^-/Na^+ and $\text{Mg}^{2+}/\text{Na}^+$ calculated from the PMF source profile were 1.79 and 0.11, respectively, similar to the corresponding ratios of the species (1.80 and 0.12, respectively) in average seawater (Ni et al., 2013). The sea salt source contributed 2.53%, 15.2% and 1.93% of OC concentrations in clusters 1 to 3, respectively, but provided no EC contribution in any of the clusters. This indicated the source consists of sea-spray organic aerosol, which came from the marine biogenic activities (Wilson et al., 2015).

The contributions of the eight sources to $\text{PM}_{2.5}$ are summarized in Table 3. The total and cluster fractional contributions (%) from each source were calculated based on the corresponding sample values simulated by PMF modeling. Amongst the eight sources, coal combustion, biomass burning and vehicle emissions were the largest contributors, which accounted for 29.6%, 19.3% and 15.9%, respectively, during the sampling period. They were followed by mineral dust (12.8%), ship emissions (8.95%), sea salt (6.58%), traffic dust (4.24%) and industrial process (2.63%) in decreasing order. Generally, the source apportionment profile of $\text{PM}_{2.5}$ in cluster 1 (BTH) was similar to that during the whole sampling period, because the regional scale pollution exhibited a pattern of atmospheric outflow of $\text{PM}_{2.5}$ mainly from the BTH region in winter (Feng et al., 2007; Feng et al., 2012). A slight increase in the contribution of vehicle emission in cluster 1 (BTH) corresponds to the great concern about vehicle emission in megacities in China (Huo et al., 2013). The source signals in cluster 2 (MON) were obviously different from that in clusters 1 (BTH) and 3 (SDP). The strong northwesterly wind in it provided more large scale spatial signals of $\text{PM}_{2.5}$ sources,

indicating that coal combustion (37.7%) and mineral dust (26.8%) were the largest contributors in north areas of China in winter. The large scale PM_{2.5} pattern linking to coal combustion agreed with the dominant position of coal consumption in Chinese energy structure. Coal consumption accounted for 66% of primary energy in China in 2014 reported by the national bureau of statistics of China (available at <http://www.stats.gov.cn/tjsj/ndsjsj/>). Other than industrial consumption, coal is additionally used for residential heating in northern areas of China during winter (Wang et al., 2013). Although the household use of coal accounts for a small portion of total coal consumption in China, its release is still a major source of PM_{2.5} in winter (Cao et al., 2012) since household stoves usually run with no or outdated environmental protection equipment. Traffic emission, of much concern in large cities, only contributed a minor part (3.57%) of PM_{2.5} on a large spatial scale because motor exhaust concentrates mainly in urban areas. In addition, biomass burning emission dominated the PM_{2.5} pollution when air masses came from the Shandong Peninsula. The abundant emission from biomass burning was mainly attributed to residential heating in the cold season (Wang et al., 2002; Hu et al., 2016).

The contributions of coal combustion, vehicle emission, industrial process, and ship emission derived from the PMF modeling of OC and EC were ranked as fossil fuel combustion for comparison. Sea salt as a marine biogenic source of OC was merged with biomass burning as contemporary carbon fractions. However, mineral dust and vehicle dust were not considered for this classification, because they originated from hybrid sources of fossil and contemporary carbon emissions. Fig. 5 shows the comparison of the PMF results and the ¹⁴C measurement.

As described in section 2.4, M1 represents the air masses from the Shandong peninsula, while M2 is on behalf of the air masses from the BTH region. In M1, the biogenic and biomass burning emission identified by PMF modeling contributed 52% to OC and 49% to EC concentrations, which were 7 and 3% below the fractions indicated by ¹⁴C measurement, respectively. The contributions of fossil fuel combustion to OC and EC from the PMF result were both 44%, which is 3 percent over and 4 percent below the corresponding values in the ¹⁴C result. Similarly, in M2, the biogenic and biomass burning emission contributed 41% to OC and 33% to EC in the PMF result, 4 and 5 percent below the ¹⁴C result, respectively. The contributions of fossil fuel combustion to OC and EC in the PMF result were 52% and 65%, respectively, which were the same percent (3%) below and over the corresponding values in the ¹⁴C result. In general, the source contributions merged from the PMF

result were lower than those from the ^{14}C measurement. This underestimation may be due to not considering the contributions of mineral dust and vehicle dust. The largest difference between PMF and ^{14}C results was 7%, indicating a minor contribution of the two sources to carbonaceous species in $\text{PM}_{2.5}$. The substantial difference was the two overestimations with the same range (3%); one was the contribution of fossil fuel combustion to OC in M1 and the other was the contribution of fossil fuel combustion to EC in M2. The overestimations were attributed to irrelevantly classifying biogenic and biomass burning emission as fossil fuel combustion. In conclusion, the minor irrelevant classification suggested that the PMF result in this study provided a reasonable source apportionment of regional $\text{PM}_{2.5}$ in North China in winter.

3.5 Implications for PM alleviation

According to the source apportionment results, coal combustion was the largest contributor of $\text{PM}_{2.5}$ in North China during winter. To alleviate PM emissions, those generated by coal combustion should be targeted first. It has been identified as the leading emission source to control in the air pollution control program. The contribution of traffic emission to $\text{PM}_{2.5}$ showed a clear spatial pattern in North China. For example, vehicle emission contributed significantly in the BTH region. Therefore, vehicle emission ought to be the second major emission source to control.

Biomass burning emission needs close attention, because it has only been lightly considered in the control program. Indeed, the first national pollution source survey demonstrated that Shandong province is the largest producer of crop stalks, such as wheat and corn, in China (Compilation-Committee-of-the-first-China-pollution-source-census, 2011). The source survey showed a production of 132 million tons in Shandong in 2007 and about 20 million tons produced in the Shandong Peninsula (including the cities of Weifang, Yantai, Weihai, Qingdao and Rizhao). Approximately 40% was household fuel for cooking and heating in the peninsula countryside. The fraction was significantly higher than in western areas of Shandong province, such as Zibo (9%) and Jinan (8%), and the fraction of open burning of crop residues in the peninsula (3%). The fraction of biomass open burning in the peninsula was also higher than its average fraction (1.5%) in Shandong province in 2007 (Compilation-Committee-of-the-first-China-pollution-source-census, 2011). Generally, emissions from agricultural field burning are mainly concentrated in the harvest season and contribute greatly to regional haze and smog events in the region, which have attracted special concern (Feng et al., 2012; Zong et al., 2015; Wang et al., 2014). Even so, open burning emission

was regarded a minor source contribution in the control program. In addition, household emission of agricultural waste, another important source for regional PM_{2.5}, is continuous or semi-continuous. It can also induce PM_{2.5} pollution on a regional scale, which has been despised or ignored (Zhang and Cao, 2015).

5 Since the 1990s, the government has enacted a series of regulations to prohibit open burning. However, it has not been fully controlled in China although its supervision is strengthened recently. The most basic reason is the lack of a reasonable alternative to utilize or dispose of huge amounts of agricultural waste each year. In the current scenario, some agricultural wastes are stored as fuel for household cooking and heating, while others are rapidly consumed by open burning in fields for the
10 next planting. Although farmers know that this disposal of agricultural residues is harmful to the environment, they still tend to do mainly due to the low costs of this method. A more permanent solution would be to find higher economic value of agricultural wastes via development of renewable techniques. In fact, agricultural wastes could be used to produce many kinds of renewable energies, such as biogas, feedstuffs, biochar, bioethanol, and bio-succinic acid. China has enacted relevant
15 energy regulations, legislation, and policy initiatives for rural renewable energy (Li et al., 2015). The government has also encouraged and sustained the renewable energy industry to increase the demand for raw feedstock. Through these efforts, China has achieved some success in renewable development in rural areas. However, these efforts are not an effective solution to the problem of surplus crop waste because the costs and benefits of renewable energy could not be offset. For
20 instance, Zhangziying, a town located in the eastern area of Beijing, has developed household biogas and straw gas since the 1980s. But renewable energy only made up approximately 10% of household energy consumption in 2011, much lower than the fraction of coal (30%) (Li et al., 2015). Before the achievement of high economic value, the government should compensate farmers for collecting crop residues as feedstock of renewable energy except for the ban on crop straw burning (Shi et al.,
25 2014a). The revenue from the subsidy and the sale of crop residues could help alleviate economic burdens on farmers, which promote them use clean energy, such as electricity, liquefied petroleum gas, biogas, etc., for household consumption (Kung and Zhang, 2015). These efforts will not only significantly improve air quality, but also make famers learn the convenience of clean energy and wake from agricultural residue burning.

30 **4 Summary and conclusion**

During the sampling period, the average PM_{2.5} concentration was $77.6 \pm 59.3 \mu\text{g m}^{-3}$, and SO₄²⁻ concentration was the highest among all constituents, with a mean of $14.2 \pm 18.0 \mu\text{g m}^{-3}$, followed by NO₃⁻ ($11.9 \pm 16.4 \mu\text{g m}^{-3}$), OC ($6.85 \pm 4.81 \mu\text{g m}^{-3}$), EC ($4.90 \pm 4.11 \mu\text{g m}^{-3}$), and NH₄⁺ ($3.11 \pm 2.14 \mu\text{g m}^{-3}$). The fractions of SO₄²⁻, NO₃⁻ and NH₄⁺ to PM_{2.5} were obviously higher than those in metropolises (e.g. Beijing and Tianjin) within North China, while fractions of carbonaceous species were markedly lower; these showed regional pollution signals.

More than half of air masses during the sampling period were from the BTH region, followed by air masses from Mongolia (35%) and the Shandong Peninsula (11%). The concentrations of PM_{2.5} and most of the species carried by air masses from the BTH region and the Shandong Peninsula were comparable ($p > 0.05$), and they occurred in statistically greater concentrations than those carried by the air masses from Mongolia ($p < 0.01$). The PM_{2.5} had an obvious signal of biomass burning emission, characterized by a high OC/EC ratio, low NO₃⁻/nss-SO₄²⁻ ratio and high nss-K⁺ concentration for the air masses coming from the Shandong Peninsula. In contrast, the PM_{2.5} tested from the BTH region showed vehicle emission pattern, characterized by low OC/EC ratio, high NO₃⁻/nss-SO₄²⁻ ratio and low nss-K⁺ concentration. This finding was confirmed by the ¹⁴C measurement of OC and EC in two merged samples selected from a successive synoptic process. The ¹⁴C measurement indicated that biogenic and biomass burning emission contributed $59 \pm 4\%$ and $52 \pm 2\%$ of OC and EC concentrations when air masses were from the Shandong Peninsula, and the contributions fell to $46 \pm 4\%$ and $38 \pm 1\%$, respectively, when the prevailing wind changed and came from the BTH region.

Based on the PMF modeling result, eight main source factors were identified. The source contributions of OC and EC from PMF for the two merged samples were compared with those indicated by the ¹⁴C measurement. Two minor overestimations with the same range (3%) showed the excellent capacity of the model, suggesting that the PMF result provided a reasonable source apportionment of regional PM_{2.5} in this study. The PMF result indicated that coal combustion, biomass burning and vehicle emissions were the largest contributors of PM_{2.5}, accounting for 29.6%, 19.3% and 15.8% of PM_{2.5}, respectively, during the sampling period. Compared with overall source apportionment result, the contribution of vehicle emission increased slightly when air masses came from the BTH region, the fraction of mineral dust and coal combustion rose clearly when air masses with high speed were from Mongolia, and biomass burning became the dominant contributor when

air masses were from the Shandong Peninsula. Biomass burning emission was highlighted in the present study, because coal combustion and vehicle emission have already been considered as major emission sources in the government air pollution control program. Before the achievement of high economic value of biomass, the government should compensate farmers for collecting them. The subsidy could help alleviate economic burdens on farmers and promote them use clean energy, which will significantly improve air quality.

Furthermore, the present study proposed that the minimum deviation between the results from PMF model and ^{14}C measurement could be employed as a criterion to select a more reliable solution for source apportionment of $\text{PM}_{2.5}$. This method can also be applied to CMB models or other isotopes (e.g. ^{13}C , ^{15}N and ^{35}S), which will help to improve scientific significance.

Acknowledgment

This work was supported by the CAS Strategic Priority Research Program (Nos. XDA11020402, XDB05030303 and XDB05040503), and the Natural Scientific Foundation of China (Nos. 41471413, 41430645 and 41373131). The authors gratefully acknowledge the National Oceanic and Atmospheric Administration's Air Resources Laboratory for providing the HYSPLIT transport model and the READY website (<http://www.arl.noaa.gov/ready.html>).

Notes

The authors declare no competing financial interest.

Reference

- Amil, N., Latif, M. T., Khan, M. F., and Mohamad, M.: Seasonal variability of $\text{PM}_{2.5}$ composition and sources in the Klang Valley urban-industrial environment, *Atmos. Chem. Phys.*, 16, 5357-5381, doi: 10.5194/acp-16-5357-2016, 2016.
- Balachandran, S., Chang, H. H., Pachon, J. E., Holmes, H. A., Mulholland, J. A., and Russell, A. G.: Bayesian-based ensemble source apportionment of $\text{PM}_{2.5}$, *Environ. Sci. Technol.*, 47, 13511-13518, doi: 10.1021/es4020647, 2013.

- Boynard, A., Clerbaux, C., Clarisse, L., Safieddine, S., Pommier, M., Van Damme, M., Bauduin, S., Oudot, C., Hadji-Lazaro, J., Hurtmans, D., and Coheur, P.-F.: First simultaneous space measurements of atmospheric pollutants in the boundary layer from IASI: A case study in the North China Plain, *Geophys. Res. Lett.*, 41, 645-651, doi: 10.1002/2013gl058333, 2014.
- 5 Bressi, M., Sciare, J., Gherzi, V., Mihalopoulos, N., Petit, J. E., Nicolas, J. B., Moukhtar, S., Rosso, A., Féron, A., Bonnaire, N., Poulakis, E., and Theodosi, C.: Sources and geographical origins of fine aerosols in Paris (France), *Atmos. Chem. Phys.*, 14, 8813-8839, doi: 10.5194/acp-14-8813-2014, 2014.
- Cao, J.-j., Chow, J. C., Tao, J., Lee, S.-c., Watson, J. G., Ho, K.-f., Wang, G.-h., Zhu, C.-s., and Han, Y.-m.: Stable carbon isotopes in aerosols from Chinese cities: Influence of fossil fuels, *Atmos. Environ.*, 45, 10 1359-1363, doi: 10.1016/j.atmosenv.2010.10.056, 2011.
- Cao, J.-J., Shen, Z.-X., Chow, J. C., Watson, J. G., Lee, S.-C., Tie, X.-X., Ho, K.-F., Wang, G.-H., and Han, Y.-M.: Winter and summer PM_{2.5} chemical compositions in fourteen Chinese cities, *J. Air Waste Manage. Assoc.*, 62, 1214-1226, doi: 10.1080/10962247.2012.701193, 2012.
- Cappa, C. D., Williams, E. J., Lack, D. A., Buffaloe, G. M., Coffman, D., Hayden, K. L., Herndon, S. C., 15 Lerner, B. M., Li, S. M., Massoli, P., McLaren, R., Nuaaman, I., Onasch, T. B., and Quinn, P. K.: A case study into the measurement of ship emissions from plume intercepts of the NOAA ship Miller Freeman, *Atmos. Chem. Phys.*, 14, 1337-1352, doi: 10.5194/acp-14-1337-2014, 2014.
- Chang, Y., Zou, Z., Deng, C., Huang, K., Collett, J. L., Lin, J., and Zhuang, G.: The importance of vehicle emissions as a source of atmospheric ammonia in the megacity of Shanghai, *Atmos. Chem. Phys.*, 16, 20 3577-3594, doi: 10.5194/acp-16-3577-2016, 2016.
- Chen, B., Andersson, A., Lee, M., Kirillova, E. N., Xiao, Q., Kruså M., Shi, M., Hu, K., Lu, Z., Streets, D. G., Du, K., and Gustafsson, Ö.: Source forensics of black carbon aerosols from China, *Environ. Sci. Technol.*, 47,

9102-9108, doi: 10.1021/es401599r, 2013.

Chinese-State-Council: Atmospheric Pollution Prevention and Control Action Plan, http://www.gov.cn/zwggk/2013-09/12/content_2486773.htm (in Chinese), access: 12, September, 2013.

5 Choi, J.-k., Heo, J.-B., Ban, S.-J., Yi, S.-M., and Zoh, K.-D.: Source apportionment of PM_{2.5} at the coastal area in Korea, *Sci. Total Environ.*, 447, 370-380, doi: 10.1016/j.scitotenv.2012.12.047, 2013.

Chow, J. C., and Watson, J. G.: Review of PM_{2.5} and PM₁₀ apportionment for fossil fuel combustion and other sources by the chemical mass balance receptor model, *Energy Fuels*, 16, 222-260, doi: 10.1021/ef0101715, 2002.

10 Chow, J. C., Watson, J. G., Chen, L. W. A., Chang, M. C. O., Robinson, N. F., Trimble, D., and Kohl, S.: The IMPROVE_A temperature protocol for thermal/optical carbon analysis: Maintaining consistency with a long-term database, *J. Air Waste Manage. Assoc.*, 57, 1014-1023, doi: 10.3155/1047-3289.57.9.1014, 2007.

Compilation-Committee-of-the-first-China-pollution-source-census: Dataset of the first China pollution source census, China Environmental Science Press, Beijing, 120 pp., 2011.

15 Cui, M., Chen, Y., Tian, C., Zhang, F., Yan, C., and Zheng, M.: Chemical composition of PM_{2.5} from two tunnels with different vehicular fleet characteristics, *Sci. Total Environ.*, 550, 123-132, doi: <http://dx.doi.org/10.1016/j.scitotenv.2016.01.077>, 2016.

Ding, X., Wang, X., Xie, Z., Zhang, Z., and Sun, L.: Impacts of siberian biomass burning on organic aerosols over the north pacific ocean and the arctic: Primary and secondary organic tracers, *Environ. Sci. Technol.*, 47, 3149-3157, doi: 10.1021/es3037093, 2013.

20 Dorado, M. P., Ballesteros, E., Arnal, J. M., Gomez, J., and Lopez, F. J.: Exhaust emissions from a Diesel engine fueled with transesterified waste olive oil, *Fuel*, 82, 1311-1315, doi: 10.1016/s0016-2361(03)00034-6, 2003.

- Du, Z., He, K., Cheng, Y., Duan, F., Ma, Y., Liu, J., Zhang, X., Zheng, M., and Weber, R.: A yearlong study of water-soluble organic carbon in Beijing I: Sources and its primary vs. secondary nature, *Atmos. Environ.*, 92, 514-521, doi: 10.1016/j.atmosenv.2014.04.060, 2014.
- Duan, J., and Tan, J.: Atmospheric heavy metals and Arsenic in China: Situation, sources and control policies, *Atmos. Environ.*, 74, 93-101, doi: 10.1016/j.atmosenv.2013.03.031, 2013.
- Feng, J., Guo, Z., Chan, C. K., and Fang, M.: Properties of organic matter in PM_{2.5} at Changdao Island, China—A rural site in the transport path of the Asian continental outflow, *Atmos. Environ.*, 41, 1924-1935, doi: 10.1016/j.atmosenv.2006.10.064, 2007.
- Feng, J., Guo, Z. G., Zhang, T. R., Yao, X. H., Chan, C. K., and Fang, M.: Source and formation of secondary particulate matter in PM_{2.5} in Asian continental outflow, *J. Geophys. Res.*, 117, D03302, doi: 10.1029/2011jd016400, 2012.
- Gelencser, A., May, B., Simpson, D., Sanchez-Ochoa, A., Kasper-Giebl, A., Puxbaum, H., Caseiro, A., Pio, C., and Legrand, M.: Source apportionment of PM_{2.5} organic aerosol over Europe: Primary/secondary, natural/anthropogenic, and fossil/biogenic origin, *J. Geophys. Res. Atmos.*, 112, doi: 10.1029/2006jd008094, 2007.
- Gibson, M. D., Pierce, J. R., Waugh, D., Kuchta, J. S., Chisholm, L., Duck, T. J., Hopper, J. T., Beauchamp, S., King, G. H., Franklin, J. E., Leitch, W. R., Wheeler, A. J., Li, Z., Gagnon, G. A., and Palmer, P. I.: Identifying the sources driving observed PM_{2.5} temporal variability over Halifax, Nova Scotia, during BORTAS-B, *Atmos. Chem. Phys.*, 13, 7199-7213, doi: 10.5194/acp-13-7199-2013, 2013.
- Gu, J., Bai, Z., Li, W., Wu, L., Liu, A., Dong, H., and Xie, Y.: Chemical composition of PM_{2.5} during winter in Tianjin, China, *Particuology*, 9, 215-221, doi: 10.1016/j.partic.2011.03.001, 2011.
- Gu, J., Du, S., Han, D., Hou, L., Yi, J., Xu, J., Liu, G., Han, B., Yang, G., and Bai, Z.-P.: Major chemical

- compositions, possible sources, and mass closure analysis of PM_{2.5} in Jinan, China, *Air Qual. Atmos. Health*, 7, 251-262, doi: 10.1007/s11869-013-0232-9, 2014.
- Gupta, D., Kim, H., Park, G., Li, X., Eom, H. J., and Ro, C. U.: Hygroscopic properties of NaCl and NaNO₃ mixture particles as reacted inorganic sea-salt aerosol surrogates, *Atmos. Chem. Phys.*, 15, 3379-3393, doi: 10.5194/acp-15-3379-2015, 2015.
- Han, S.-q., Wu, J.-h., Zhang, Y.-f., Cai, Z.-y., Feng, Y.-c., Yao, Q., Li, X.-j., Liu, Y.-w., and Zhang, M.: Characteristics and formation mechanism of a winter haze–fog episode in Tianjin, China, *Atmos. Environ.*, 98, 323-330, doi: 10.1016/j.atmosenv.2014.08.078, 2014.
- Hu, M., Guo, S., Peng, J.-f., and Wu, Z.-j.: Insight into characteristics and sources of PM_{2.5} in the Beijing–Tianjin–Hebei region, China, *Natl. Sci. Rev.*, 2, 257-258, doi: 10.1093/nsr/nwv003, 2015.
- Hu, W., Hu, M., Hu, W., Jimenez, J. L., Yuan, B., Chen, W., Wang, M., Wu, Y., Chen, C., Wang, Z., Peng, J., Zeng, L., and Shao, M.: Chemical composition, sources, and aging process of submicron aerosols in Beijing: Contrast between summer and winter, *J. Geophys. Res.*, 121, 1955-1977, doi: 10.1002/2015jd024020, 2016.
- Huang, R.-J., Zhang, Y., Bozzetti, C., Ho, K.-F., Cao, J.-J., Han, Y., Daellenbach, K. R., Slowik, J. G., Platt, S. M., Canonaco, F., Zotter, P., Wolf, R., Pieber, S. M., Bruns, E. A., Crippa, M., Ciarelli, G., Piazzalunga, A., Schwikowski, M., Abbaszade, G., Schnelle-Kreis, J., Zimmermann, R., An, Z., Szidat, S., Baltensperger, U., Haddad, I. E., and Prevot, A. S. H.: High secondary aerosol contribution to particulate pollution during haze events in China, *Nature*, 514, 218–222, doi: 10.1038/nature13774, 2014.
- Huo, H., Zhang, Q., Liu, F., and He, K.: Climate and environmental effects of electric vehicles versus compressed natural gas vehicles in China: A life-cycle analysis at provincial level, *Environ. Sci. Technol.*, 47, 1711-1718, doi: 10.1021/es303352x, 2013.
- Jing, B., Wu, L., Mao, H., Gong, S., He, J., Zou, C., Song, G., Li, X., and Wu, Z.: Development of a vehicle

- emission inventory with high temporal-spatial resolution based on NRT traffic data and its impact on air pollution in Beijing - Part 1: Development and evaluation of vehicle emission inventory, *Atmos. Chem. Phys.*, 16, 3161-3170, doi: 10.5194/acp-16-3161-2016, 2016.
- Kessler, R.: Prevention: Air of danger, *Nature*, 509, S62-S63, doi: 10.1038/509S62a, 2014.
- 5 Khan, M. F., Latif, M. T., Saw, W. H., Amil, N., Nadzir, M. S. M., Sahani, M., Tahir, N. M., and Chung, J. X.: Fine particulate matter in the tropical environment: monsoonal effects, source apportionment, and health risk assessment, *Atmos. Chem. Phys.*, 16, 597-617, doi: 10.5194/acp-16-597-2016, 2016.
- Kung, C.-C., and Zhang, N.: Renewable energy from pyrolysis using crops and agricultural residuals: An economic and environmental evaluation, *Energy*, 90, Part 2, 1532-1544, doi: 10.1016/j.energy.2015.06.114,
10 2015.
- Levin, I., Naegler, T., Kromer, B., Diehl, M., Francey, R. J., Gomez-Pelaez, A. J., Steele, L. P., Wagenbach, D., Weller, R., and Worthy, D. E.: Observations and modelling of the global distribution and long-term trend of atmospheric $^{14}\text{CO}_2$, *Tellus Ser. B*, 62, 26-46, doi: 10.1111/j.1600-0889.2009.00446.x, 2010.
- Li, X., Lin, C., Wang, Y., Zhao, L., Duan, N., and Wu, X.: Analysis of rural household energy consumption
15 and renewable energy systems in Zhangziying town of Beijing, *Ecol. Modell.*, 318, 184-193, doi: 10.1016/j.ecolmodel.2015.05.011, 2015.
- Liu, D., Li, J., Zhang, Y., Xu, Y., Liu, X., Ding, P., Shen, C., Chen, Y., Tian, C., and Zhang, G.: The use of levoglucosan and radiocarbon for source apportionment of $\text{PM}_{2.5}$ carbonaceous aerosols at a background site in East China, *Environ. Sci. Technol.*, 47, 10454-10461, doi: 10.1021/es401250k, 2013.
- 20 Liu, J., Li, J., Zhang, Y., Liu, D., Ding, P., Shen, C., Shen, K., He, Q., Ding, X., Wang, X., Chen, D., Szidat, S., and Zhang, G.: Source apportionment using radiocarbon and organic tracers for $\text{PM}_{2.5}$ carbonaceous aerosols in Guangzhou, South China: Contrasting local- and regional-scale haze events, *Environ. Sci.*

- Technol., 48, 12002-12011, doi: 10.1021/es503102w, 2014.
- Lu, F., Xu, D., Cheng, Y., Dong, S., Guo, C., Jiang, X., and Zheng, X.: Systematic review and meta-analysis of the adverse health effects of ambient PM_{2.5} and PM₁₀ pollution in the Chinese population, *Environ. Res.*, 136, 196-204, doi: <http://dx.doi.org/10.1016/j.envres.2014.06.029>, 2015.
- 5 Mohn, J., Szidat, S., Fellner, J., Rechberger, H., Quartier, R., Buchmann, B., and Emmenegger, L.: Determination of biogenic and fossil CO₂ emitted by waste incineration based on (CO₂)-C-14 and mass balances, *Bioresour. Technol.*, 99, 6471-6479, doi: 10.1016/j.biortech.2007.11.042, 2008.
- Ni, T., Li, P., Han, B., Bai, Z., Ding, X., Wang, Q., Huo, J., and Lu, B.: Spatial and Temporal Variation of Chemical Composition and Mass Closure of Ambient PM₁₀ in Tianjin, China, *Aerosol Air Qual. Res.*, 13, 10 1832-1846, doi: 10.4209/aaqr.2012.10.0283, 2013.
- Paatero, P., and Tapper, U.: Positive matrix factorization: A non-negative factor model with optimal utilization of error estimates of data values, *Environmetrics*, 5, 111-126, doi: 10.1002/env.3170050203, 1994.
- Paatero, P., Eberly, S., Brown, S. G., and Norris, G. A.: Methods for estimating uncertainty in factor analytic solutions, *Atmos. Meas. Tech.*, 7, 781-797, doi: 10.5194/amt-7-781-2014, 2014.
- 15 Pan, Y., Wang, Y., Sun, Y., Tian, S., and Cheng, M.: Size-resolved aerosol trace elements at a rural mountainous site in Northern China: Importance of regional transport, *Sci. Total Environ.*, 461-462, 761-771, doi: 10.1016/j.scitotenv.2013.04.065, 2013.
- Pey, J., Pérez, N., Cortés, J., Alastuey, A., and Querol, X.: Chemical fingerprint and impact of shipping emissions over a western Mediterranean metropolis: Primary and aged contributions, *Sci. Total Environ.*, 20 463-464, 497-507, doi: 10.1016/j.scitotenv.2013.06.061, 2013.
- Pui, D. Y. H., Chen, S.-C., and Zuo, Z.: PM_{2.5} in China: Measurements, sources, visibility and health effects, and mitigation, *Particuology*, 13, 1-26, doi: 10.1016/j.partic.2013.11.001, 2014.

- Shahsavani, A., Naddafi, K., Jaafarzadeh Haghighifard, N., Mesdaghinia, A., Yunesian, M., Nabizadeh, R., Arhami, M., Yarahmadi, M., Sowlat, M. H., Ghani, M., Jonidi Jafari, A., Alimohamadi, M., Motevalian, S. A., and Soleimani, Z.: Characterization of ionic composition of TSP and PM₁₀ during the Middle Eastern Dust (MED) storms in Ahvaz, Iran, *Environ. Monit. Assess.*, 184, 6683-6692, doi: 10.1007/s10661-011-2451-6, 5 2012.
- Sheehan, P., Cheng, E., English, A., and Sun, F.: China's response to the air pollution shock, *Nat. Clim. Change*, 4, 306-309, doi: 10.1038/nclimate2197, 2014.
- Shi, T., Liu, Y., Zhang, L., Hao, L., and Gao, Z.: Burning in agricultural landscapes: an emerging natural and human issue in China, *Landsc. Ecol.*, 29, 1785-1798, doi: 10.1007/s10980-014-0060-9, 2014a.
- 10 Shi, Y., Xia, Y.-f., Lu, B.-h., Liu, N., Zhang, L., Li, S.-j., and Li, W.: Emission inventory and trends of NO_x for China, 2000–2020, *J. Zhejiang Univ.-Sci.*, 15, 454-464, doi: 10.1631/jzus.A1300379, 2014b.
- Szidat, S., Jenk, T. M., Gägeler, H. W., Synal, H. A., Fisseha, R., Baltensperger, U., Kalberer, M., Samburova, V., Reimann, S., Kasper-Giebl, A., and Hajdas, I.: Radiocarbon (¹⁴C)-deduced biogenic and anthropogenic contributions to organic carbon (OC) of urban aerosols from Zürich, Switzerland, *Atmos. Environ.*, 38, 4035-4044, doi: 10.1016/j.atmosenv.2004.03.066, 2004. 15
- Szidat, S.: Sources of Asian Haze, *Science*, 323, 470-471, doi: 10.1126/science.1169407, 2009.
- Tan, J.-H., Duan, J.-C., Ma, Y.-L., Yang, F.-M., Cheng, Y., He, K.-B., Yu, Y.-C., and Wang, J.-W.: Source of atmospheric heavy metals in winter in Foshan, China, *Sci. Total Environ.*, 493, 262-270, doi: 10.1016/j.scitotenv.2014.05.147, 2014.
- 20 Tan, J., Duan, J., Zhen, N., He, K., and Hao, J.: Chemical characteristics and source of size-fractionated atmospheric particle in haze episode in Beijing, *Atmos. Res.*, 167, 24-33, doi: 10.1016/j.atmosres.2015.06.015, 2016.

- Tao, J., Gao, J., Zhang, L., Zhang, R., Che, H., Zhang, Z., Lin, Z., Jing, J., Cao, J., and Hsu, S. C.: PM_{2.5} pollution in a megacity of southwest China: source apportionment and implication, *Atmos. Chem. Phys.*, 14, 8679-8699, doi: 10.5194/acp-14-8679-2014, 2014a.
- Tao, M., Chen, L., Xiong, X., Zhang, M., Ma, P., Tao, J., and Wang, Z.: Formation process of the widespread extreme haze pollution over northern China in January 2013: Implications for regional air quality and climate, *Atmos. Environ.*, 98, 417-425, doi: <http://dx.doi.org/10.1016/j.atmosenv.2014.09.026>, 2014b.
- Tian, S., Pan, Y., Liu, Z., Wen, T., and Wang, Y.: Size-resolved aerosol chemical analysis of extreme haze pollution events during early 2013 in urban Beijing, China, *J. Hazard. Mater.*, 279, 452-460, doi: 10.1016/j.jhazmat.2014.07.023, 2014.
- 10 Tian, S. L., Pan, Y. P., and Wang, Y. S.: Size-resolved source apportionment of particulate matter in urban Beijing during haze and non-haze episodes, *Atmos. Chem. Phys.*, 16, 1-19, doi: 10.5194/acp-16-1-2016, 2016.
- Wacker, L., Fahrni, S. M., Hajdas, I., Molnar, M., Synal, H. A., Szidat, S., and Zhang, Y. L.: A versatile gas interface for routine radiocarbon analysis with a gas ion source, *Nucl. Instrum. Methods Phys. Res., Sect. B*, 294, 315-319, doi: 10.1016/j.nimb.2012.02.009, 2013.
- 15 Wang, T., Cheung, T. F., Li, Y. S., Yu, X. M., and Blake, D. R.: Emission characteristics of CO, NO_x, SO₂ and indications of biomass burning observed at a rural site in eastern China, *J. Geophys. Res.*, 107, doi: 10.1029/2001jd000724, 2002.
- Wang, X., Bi, X., Sheng, G., and Fu, J.: Hospital indoor PM₁₀/PM_{2.5} and associated trace elements in Guangzhou, China, *Sci. Total Environ.*, 366, 124-135, doi: 10.1016/j.scitotenv.2005.09.004, 2006.
- 20 Wang, X., Williams, B. J., Wang, X., Tang, Y., Huang, Y., Kong, L., Yang, X., and Biswas, P.: Characterization of organic aerosol produced during pulverized coal combustion in a drop tube furnace, *Atmos. Chem. Phys.*, 13, 10919-10932, doi: 10.5194/acp-13-10919-2013, 2013.

- Wang, X., Chen, Y., Tian, C., Huang, G., Fang, Y., Zhang, F., Zong, Z., Li, J., and Zhang, G.: Impact of agricultural waste burning in the Shandong Peninsula on carbonaceous aerosols in the Bohai Rim, China, *Sci. Total Environ.*, 481, 311-316, doi: 10.1016/j.scitotenv.2014.02.064, 2014.
- Wang, Y., Zhuang, G. S., Tang, A. H., Yuan, H., Sun, Y. L., Chen, S. A., and Zheng, A. H.: The ion chemistry and the source of PM_{2.5} aerosol in Beijing, *Atmos. Environ.*, 39, 3771-3784, doi: 10.1016/j.atmosenv.2005.03.013, 2005.
- Weber, R. J., Sullivan, A. P., Peltier, R. E., Russell, A., Yan, B., Zheng, M., de Gouw, J., Warneke, C., Brock, C., Holloway, J. S., Atlas, E. L., and Edgerton, E.: A study of secondary organic aerosol formation in the anthropogenic-influenced southeastern United States, *J. Geophys. Res. Atmos.*, 112, D13302, doi: 10.1029/2007JD008408, 2007.
- Wilson, T. W., Ladino, L. A., Alpert, P. A., Breckels, M. N., Brooks, I. M., Browse, J., Burrows, S. M., Carslaw, K. S., Huffman, J. A., Judd, C., Kilhau, W. P., Mason, R. H., McFiggans, G., Miller, L. A., Najera, J. J., Polishchuk, E., Rae, S., Schiller, C. L., Si, M., Temprado, J. V., Whale, T. F., Wong, J. P. S., Wurl, O., Yakobi-Hancock, J. D., Abbatt, J. P. D., Aller, J. Y., Bertram, A. K., Knopf, D. A., and Murray, B. J.: A marine biogenic source of atmospheric ice-nucleating particles, *Nature*, 525, 234-238, doi: 10.1038/nature14986, 2015.
- Xu, X., Trumbore, S. E., Zheng, S., Southon, J. R., McDuffee, K. E., Luttgen, M., and Liu, J. C.: Modifying a sealed tube zinc reduction method for preparation of AMS graphite targets: Reducing background and attaining high precision, *Nucl. Instrum. Methods Phys. Res., Sect. B*, 259, 320-329, doi: 10.1016/j.nimb.2007.01.175, 2007.
- Yang, F., Tan, J., Zhao, Q., Du, Z., He, K., Ma, Y., Duan, F., and Chen, G.: Characteristics of PM_{2.5} speciation in representative megacities and across China, *Atmos. Chem. Phys.*, 11, 5207-5219, doi:

10.5194/acp-11-5207-2011, 2011.

Zhang, F., Chen, Y., Tian, C., Wang, X., Huang, G., Fang, Y., and Zong, Z.: Identification and quantification of shipping emissions in Bohai Rim, China, *Sci. Total Environ.*, 497–498, 570-577, doi: 10.1016/j.scitotenv.2014.08.016, 2014a.

5 Zhang, R., Jing, J., Tao, J., Hsu, S. C., Wang, G., Cao, J., Lee, C. S. L., Zhu, L., Chen, Z., Zhao, Y., and Shen, Z.: Chemical characterization and source apportionment of PM_{2.5} in Beijing: seasonal perspective, *Atmos. Chem. Phys.*, 13, 7053-7074, doi: 10.5194/acp-13-7053-2013, 2013.

Zhang, S., Wu, Y., Wu, X., Li, M., Ge, Y., Liang, B., Xu, Y., Zhou, Y., Liu, H., Fu, L., and Hao, J.: Historic and future trends of vehicle emissions in Beijing, 1998–2020: A policy assessment for the most stringent vehicle
10 emission control program in China, *Atmos. Environ.*, 89, 216-229, doi: 10.1016/j.atmosenv.2013.12.002, 2014b.

Zhang, Y.-L., Li, J., Zhang, G., Zotter, P., Huang, R.-J., Tang, J.-H., Wacker, L., Prévôt, A. S. H., and Szidat, S.: Radiocarbon-based source apportionment of carbonaceous aerosols at a regional background site on Hainan Island, South China, *Environ. Sci. Technol.*, 48, 2651-2659, doi: 10.1021/es4050852, 2014c.

15 Zhang, Y.-L., and Cao, F.: Is it time to tackle PM_{2.5} air pollutions in China from biomass-burning emissions?, *Environ. Pollut.*, 202, 217-219, doi: 10.1016/j.envpol.2015.02.005, 2015.

Zhang, Y. L., Liu, D., Shen, C. D., Ding, P., and Zhang, G.: Development of a preparation system for the radiocarbon analysis of organic carbon in carbonaceous aerosols in China, *Nucl. Instrum. Methods Phys. Res., Sect. B*, 268, 2831-2834, doi: 10.1016/j.nimb.2010.06.032, 2010.

20 Zhang, Y. L., Huang, R. J., El Haddad, I., Ho, K. F., Cao, J. J., Han, Y., Zotter, P., Bozzetti, C., Daellenbach, K. R., Canonaco, F., Slowik, J. G., Salazar, G., Schwikowski, M., Schnelle-Kreis, J., Abbaszade, G., Zimmermann, R., Baltensperger, U., Prévôt, A. S. H., and Szidat, S.: Fossil vs. non-fossil sources of fine

- carbonaceous aerosols in four Chinese cities during the extreme winter haze episode of 2013, *Atmos. Chem. Phys.*, 15, 1299-1312, doi: 10.5194/acp-15-1299-2015, 2015.
- Zhao, B., Wang, P., Ma, J. Z., Zhu, S., Pozzer, A., and Li, W.: A high-resolution emission inventory of primary pollutants for the Huabei region, China, *Atmos. Chem. Phys.*, 12, 481-501, doi: 10.5194/acp-12-481-2012, 5 2012.
- Zhao, P. S., Dong, F., He, D., Zhao, X. J., Zhang, X. L., Zhang, W. Z., Yao, Q., and Liu, H. Y.: Characteristics of concentrations and chemical compositions for PM_{2.5} in the region of Beijing, Tianjin, and Hebei, China, *Atmos. Chem. Phys.*, 13, 4631-4644, doi: 10.5194/acp-13-4631-2013, 2013.
- Zheng, B., Huo, H., Zhang, Q., Yao, Z. L., Wang, X. T., Yang, X. F., Liu, H., and He, K. B.: High-resolution mapping of vehicle emissions in China in 2008, *Atmos. Chem. Phys.*, 14, 9787-9805, doi: 10 10.5194/acp-14-9787-2014, 2014.
- Zhou, J. B., Xing, Z. Y., Deng, J. J., and Du, K.: Characterizing and sourcing ambient PM_{2.5} over key emission regions in China I: Water-soluble ions and carbonaceous fractions, *Atmos. Environ.*, 135, 20-30, doi: 10.1016/j.atmosenv.2016.03.054, 2016.
- 15 Zhou, Y., Cheng, S., Lang, J., Chen, D., Zhao, B., Liu, C., Xu, R., and Li, T.: A comprehensive ammonia emission inventory with high-resolution and its evaluation in the Beijing–Tianjin–Hebei (BTH) region, China, *Atmos. Environ.*, 106, 305-317, doi: 10.1016/j.atmosenv.2015.01.069, 2015.
- Zong, Z., Chen, Y., Tian, C., Fang, Y., Wang, X., Huang, G., Zhang, F., Li, J., and Zhang, G.: Radiocarbon-based impact assessment of open biomass burning on regional carbonaceous aerosols in North 20 China, *Sci. Total Environ.*, 518–519, 1-7, doi: 10.1016/j.scitotenv.2015.01.113, 2015.

Table 1. Statistics of PM_{2.5} chemical species in different clusters and significant level by mean test

Species (unit)	Mean \pm standard deviation (range)			Significant level		
	Cluster1(n=42)	Cluster2(n=25)	Cluster3(n=9)	1&2	1&3	2&3
PM _{2.5} ($\mu\text{g m}^{-3}$)	93.0 \pm 66.1 (24.5–305)	41.6 \pm 26.7 (12.7–143)	106 \pm 42.3 (50.3–193)	0.00	0.59	0.00
EC ($\mu\text{g m}^{-3}$)	6.53 \pm 4.66 (1.39–19.6)	2.50 \pm 1.84 (0.800–8.85)	3.94 \pm 1.49 (2.53–7.66)	0.00	0.11	0.05
OC ($\mu\text{g m}^{-3}$)	8.58 \pm 5.23 (1.45–21.3)	3.51 \pm 2.35 (0.810–11.4)	8.04 \pm 2.32 (5.25–13.5)	0.00	0.76	0.00
Cl ⁻ ($\mu\text{g m}^{-3}$)	2.37 \pm 2.11 (0.100–8.90)	1.22 \pm 0.650 (0.200–2.85)	2.94 \pm 1.35 (1.42–5.53)	0.01	0.45	0.00
NO ₃ ⁻ ($\mu\text{g m}^{-3}$)	17.6 \pm 19.6 (1.75–87.0)	2.75 \pm 4.25 (0.270–20.1)	10.6 \pm 6.09 (4.41–20.3)	0.00	0.30	0.00
SO ₄ ²⁻ ($\mu\text{g m}^{-3}$)	19.4 \pm 21.8 (2.09–96.2)	4.55 \pm 4.06 (1.37–19.5)	16.4 \pm 8.74 (5.34–35.6)	0.00	0.69	0.00
Na ⁺ ($\mu\text{g m}^{-3}$)	0.380 \pm 0.240 (0.05–1.58)	0.550 \pm 0.260 (0.180–1.08)	0.310 \pm 0.06 (0.220–0.400)	0.01	0.41	0.01
NH ₄ ⁺ ($\mu\text{g m}^{-3}$)	3.97 \pm 2.29 (1.28–10.1)	1.53 \pm 0.980 (0.610–4.70)	3.52 \pm 0.96 (1.93–4.90)	0.00	0.57	0.00
K ⁺ ($\mu\text{g m}^{-3}$)	1.11 \pm 0.740 (0.28–3.10)	0.350 \pm 0.360 (0.07–1.69)	2.01 \pm 0.93 (0.780–3.95)	0.00	0.00	0.00
Mg ²⁺ ($\mu\text{g m}^{-3}$)	0.03 \pm 0.03 (0.01–0.17)	0.03 \pm 0.02 (0.01–0.11)	0.02 \pm 0.01 (0.01–0.04)	0.66	0.41	0.13
Ca ²⁺ ($\mu\text{g m}^{-3}$)	0.370 \pm 0.220 (0.110–1.32)	0.370 \pm 0.180 (0.07–0.74)	0.440 \pm 0.290 (0.09–0.97)	1.00	0.46	0.46
Ti (ng m ⁻³)	6.96 \pm 5.98 (0.350–25.9)	10.9 \pm 9.10 (0.01–30.7)	2.51 \pm 0.85 (1.16–3.58)	0.04	0.03	0.01
V (ng m ⁻³)	4.68 \pm 2.29 (0.760–11.3)	2.83 \pm 2.55 (0.450–12.4)	3.24 \pm 1.50 (2.05–7.12)	0.00	0.08	0.66
Mn (ng m ⁻³)	33.8 \pm 31.3 (1.97–108)	17.6 \pm 19.3 (1.38–95.4)	40.9 \pm 20.3 (9.14–69.8)	0.02	0.53	0.01
Fe (ng m ⁻³)	404 \pm 308 (7.12–1588)	375 \pm 263 (9.13–826)	521 \pm 188 (244–960)	0.70	0.29	0.15
Co (ng m ⁻³)	0.260 \pm 0.200 (0.01–0.73)	0.170 \pm 0.140 (0.01–0.48)	0.360 \pm 0.130 (0.100–0.590)	0.08	0.14	0.00
Ni (ng m ⁻³)	4.85 \pm 2.56 (1.68–13.8)	3.51 \pm 1.85 (1.68–6.79)	3.80 \pm 1.02 (2.45–5.84)	0.03	0.24	0.67
Cu (ng m ⁻³)	11.6 \pm 13.6 (0.720–77.7)	3.06 \pm 2.93 (0.03–8.99)	13.9 \pm 7.05 (3.90–26.4)	0.00	0.64	0.00
Zn (ng m ⁻³)	146 \pm 176 (9.92–987)	46.4 \pm 50.1 (5.56–208)	90.4 \pm 47.4 (24.2–201)	0.01	0.36	0.03
As (ng m ⁻³)	9.03 \pm 9.52 (1.11–43.4)	3.00 \pm 2.82 (0.67–14.0)	5.35 \pm 3.35 (2.25–13.6)	0.00	0.27	0.06
Cd (ng m ⁻³)	2.70 \pm 5.26 (0.110–25.9)	0.450 \pm 0.410 (0.04–1.29)	1.54 \pm 0.65 (0.490–2.66)	0.04	0.52	0.00
Pb (ng m ⁻³)	110 \pm 95.3 (5.30–412)	36.9 \pm 44.8 (3.02–176)	128 \pm 53.2 (45.4–215)	0.00	0.59	0.00

Table 2. Concentration and contemporary carbon fraction of carbonaceous species in M1 and M2

	M1	M2		M1	M2
PM _{2.5} ($\mu\text{g m}^{-3}$)	159 \pm 0.510	91.8 \pm 0.490			
OC ($\mu\text{g m}^{-3}$)	12.7 \pm 0.700	9.01 \pm 0.510	f_c (OC)	0.59 \pm 0.04	0.46 \pm 0.04
WSOC ($\mu\text{g m}^{-3}$)	6.42 \pm 0.410	3.70 \pm 0.200	f_c (WSOC)	0.59 \pm 0.03	0.49 \pm 0.03
WIOC ($\mu\text{g m}^{-3}$)	6.30 \pm 0.620	5.31 \pm 0.400	f_c (WIOC)	0.60 \pm 0.03	0.43 \pm 0.03
EC ($\mu\text{g m}^{-3}$)	8.60 \pm 0.500	5.80 \pm 0.310	f_c (EC)	0.52 \pm 0.02	0.38 \pm 0.01

5

Table 3. Averages of fractional contributions (%) from eight sources identified by PMF model

	Vehicle emission	Traffic dust	Ship emission	Industrial process	Biomass burning	Mineral dust	Coal combustion	Sea salt
All	15.9	4.24	8.95	2.63	19.3	12.8	29.6	6.58
Cluster1	23.6	4.89	8.79	3.64	19.6	6.32	29.2	3.96
Cluster2	3.57	3.60	9.35	1.20	4.88	26.8	37.7	12.9
Cluster3	12.4	3.08	8.67	1.96	52.7	6.46	12.4	2.33

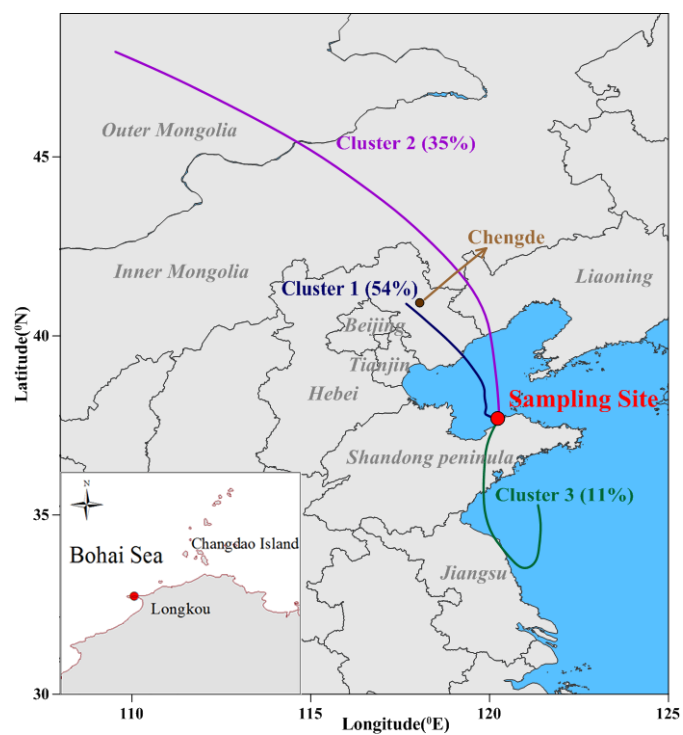


Figure 1. The sampling site and 48-h back trajectory clusters during the sampling period



Figure 2. 48-h back trajectories with 12 h intervals of the combined samples (M1 and M2) selected for ^{14}C analysis. M1 were collected continually from 06:00 to 18:00, 16th January and from 18:00 to 06:00 the next day, when the air masses were derived from the south and passed through the Shandong Peninsula; M2 were collected continually from 17th January 18:00 to 6:00 and from 06:00 to 18:00 in the next day, when the air masses come from the north and reflected the BTH pattern. (The digit in the figure is date and time with the format of YYYYMMDDHH, the time is local time).

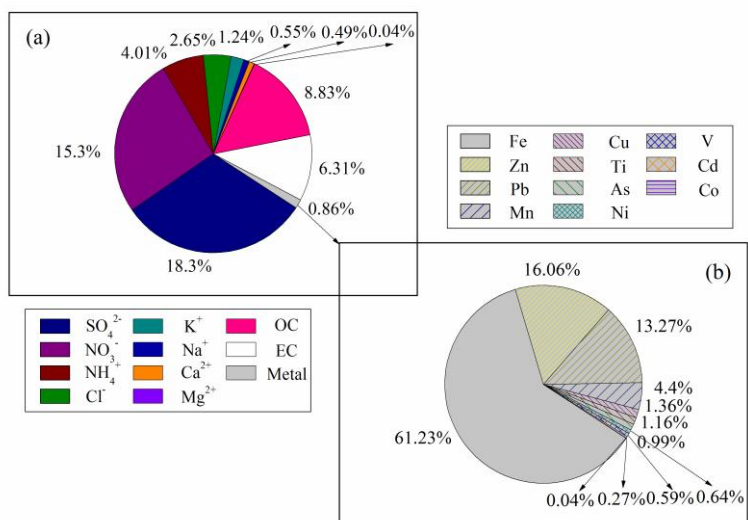


Figure 3. Pie-charts showing the relative contribution of species for PM_{2.5} in Qimu Island. Note the sum of percentage of identified species in PM_{2.5} in (a) is 58.58%, while that of (b) is 100% because the percentage is the ratio of every mental element to the total identified mental elements.

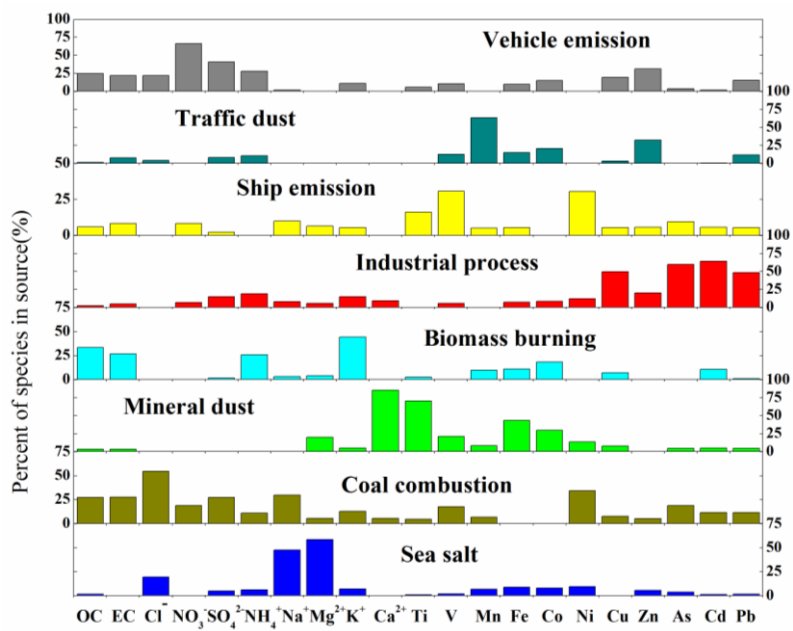


Figure 4. The contribution profiles of eight sources identified by PMF model

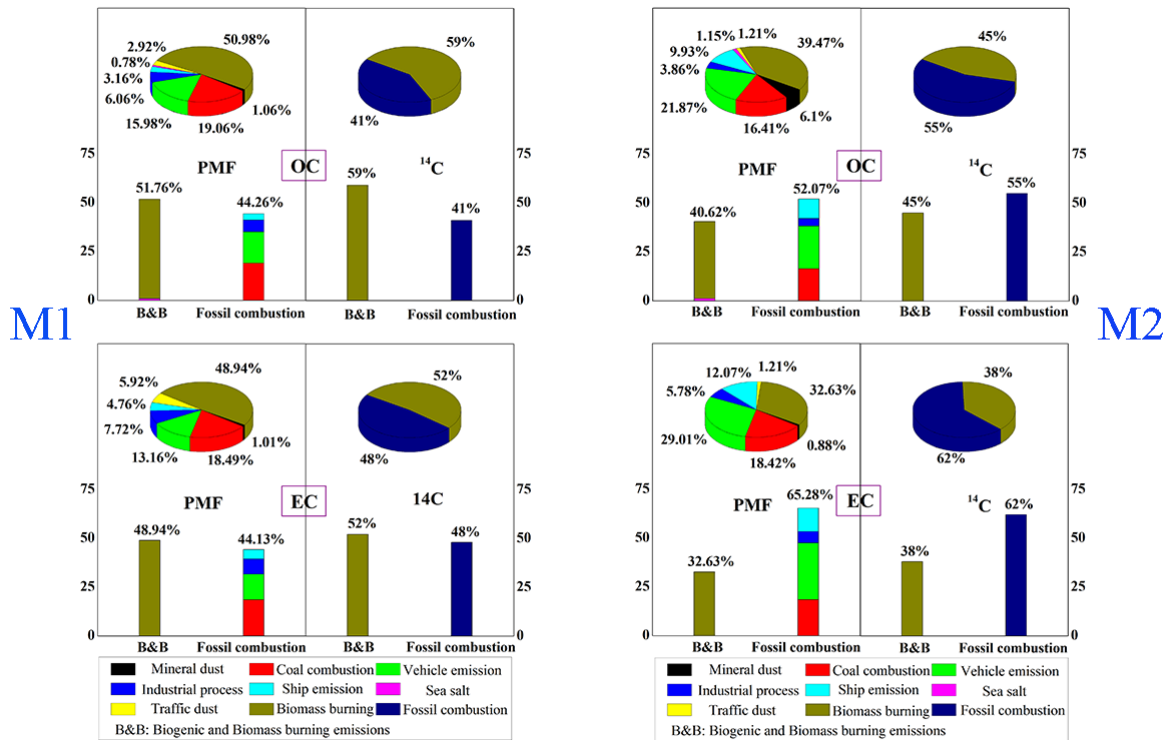


Figure 5. Comparison of source apportionment of OC and EC in the two specified samples (M1 and M2) from PMF and ¹⁴C measurement. B&B refers to the source of biogenic and biomass burning. Note: the B&B and Fossil emissions from the PMF result do not add to a hundred in the bars because hybrid sources from B&B and fossil fuel combustion were not be considered in the comparison (mineral dust and vehicle dust).